Imaging highly confined modes in sub-micron scale silicon waveguides using Transmission-based Near-field Scanning Optical Microscopy

Jacob T. Robinson, Stefan F. Preble, Michal Lipson

Department of Electrical and Computer Engineering, Cornell University Ithaca, NY 14853
ml292@cornell.edu

Abstract: We demonstrate a new technique for high resolution imaging of near field profiles in highly confining photonic structures. This technique, Transmission-based Near-field Scanning Optical Microscopy (TraNSOM), measures changes in transmission through a waveguide resulting from near field perturbation by a scanning metallic probe. Using this technique we compare different mode polarizations and measure a transverse optical decay length of λ/15 in sub-micron Silicon On Insulator (SOI) waveguides. These measurements compare well to theoretical results.

OCIS codes: (180.5810) Scanning microscopy; (130.2790) Guided waves; (130.5990) Semiconductor integrated optics; (130.3060) Infrared integrated optics; (290.220) Scattering extinction; (999.9999) Near-field optics.

References and links

1. B. Jalali, et al., "Advances in silicon-on-insulator optoelectronics," IEEE J. Sel. Top. Quantum Electron. **4**, 938947 (1998).
2. V.R. Almeida, C.A. Barrios, R.R. Panepucci, and M. Lipson, "All-optical control of light on a silicon chip," Nature **431**, 1081-1084 (2004).
3. Q. Xu, B. Schmidt, S. Pradhan, and M. Lipson, "Micrometre-scale silicon electro-optic modulator," Nature **435**, 325-327 (2005).
4. A. Liu, et al., "A high-speed silicon optical modulator based on a metal-oxide-semiconductor capacitor," Nature **427**, 615-618 (2004).
5. T. Tanabe, M. Notomi, S. Mitsugi, A. Shinya, and E. Kuramochi, "Fast bistable all-optical switch and memory on a silicon photonic crystal on-chip," Opt. Lett. **30**, 2575-2577 (2005).
6. Y.A. Vlasov, M. O'Boyle, H.F. Hamann, and S.J. McNab, "Active control of slow light on a chip with photonic crystal waveguides," Nature **438**, 65-69 (2005).
7. Y. Okawachi, et al., "All-optical slow-light on a photonic chip," Opt. Express **14**, 2317-2322 (2006), http://www.opticsinfobase.org/abstract.cfm?URI=oe-14-6-2317.
8. H. Rong, et al., "Raman gain and nonlinear optical absorption measurements in a low-loss silicon waveguide," App. Phys. Lett. **85**, 2196-2198 (2004).
9. Q. Xu, V.R. Almeida, and M. Lipson, "Time-resolved study of raman gain in highly confined silicon-on-insulator waveguides," Opt. Express **12**, 4437 (2004), http://www.opticsinfobase.org/abstract.cfm?URI=oe-12-19-4437.
10. R.L. Espinola, J.I. Dadap, R.M. Osgood, Jr., S.J. McNab, and Y.A. Vlasov, "Raman amplification in ultrasmall silicon-on-insulator wire waveguides," Opt. Express **12**, 3713 (2004), http://www.opticsinfobase.org/abstract.cfm?URI=oe-12-16-3713.
11. R. Naisheng, et al., "A continuous-wave raman silicon laser," Nature **433**, 725-728 (2005).
12. O. Boyraz and B. Jalali, "Demonstration of directly modulated silicon raman laser," Opt. Express **13**, 796 (2005), http://www.opticsinfobase.org/abstract.cfm?URI=oe-13-3-796.
13. M.A. Foster, et al., "Broad-band optical parametric gain on a silicon photonic chip," Nature **441**, 960-963 (2006).
14. S. Bourzeix, et al., "Near-field optical imaging of light propagation in semiconductor waveguide structures," App. Phys. Lett. **73**, 1035-1037 (1998).
15. B. Hecht, et al., "Scanning near-field optical microscopy with aperture probes: Fundamentals and applications," J. Chem. Phys. **112**, 7761-7774 (2000).

#75030 - $15.00 USD Received 14 September 2006; revised 5 October 2006; accepted 6 October 2006

16. C.D. Poweleit, D.H. Naghski, S.M. Lindsay, J.T. Boyd, and H.E. Jackson, "Near field scanning optical microscopy measurements of optical intensity distributions in semiconductor channel waveguides," App. Phys. Lett. **69**, 3471-3473 (1996).
17. G.H. Vander Rhodes, et al., "Measurement of internal spatial modes and local propagation properties in optical waveguides," App. Phys. Lett. **75**, 2368-2370 (1999).
18. H.A. Bethe, "Theory of diffraction by small holes," Phys. Rev. **66**, 163 (1944).
19. R. Bachelot, P. Gleyzes, and A.C. Boccara, "Near-field optical microscope based on local perturbation of a diffraction spot," Opt. Lett. **20**, 1924-1926 (1995).
20. Y. Inouye and S. Kawata, "Near-field scanning optical microscope with a metallic probe tip," Opt. Lett. **19**, 159-161 (1994).
21. R. Bachelot, et al., "Probing photonic and optoelectronic structures by apertureless scanning near-field optical microscopy," Microsc. Res. Tech. **64**, 441-452 (2004).
22. L. Gomez, et al., "Apertureless scanning near-field optical microscopy: A comparison between homodyne and heterodyne approaches," J. Opt. Soc. Am. B **23**, 823-833 (2006).
23. I. Stefanon, et al., "Heterodyne detection of guided waves using a scattering-type scanning near-field optical microscope," Opt. Express **13**, (2005).
24. M.L.M. Balistreri, H. Gersen, J.P. Korterik, L. Kuipers, and N.F. van Hulst, "Tracking femtosecond laser pulses in space and time," Science **294**, 1080-1082 (2001).
25. W.C.L. Hopman, et al., "Nano-mechanical tuning and imaging of a photonic crystal micro-cavity resonance," Opt. Express **14**, 8745-8752 (2006), http://www.opticsinfobase.org/abstract.cfm?URI=oe-14-19-8745.
26. V.R. Almeida, R.R. Panepucci, and M. Lipson, "Nanotaper for compact mode conversion," Opt. Lett. **28**, 1302-1304 (2003).
27. S.J. McNab, N. Moll, and Y.A. Vlasov, "Ultra-low loss photonic integrated circuit with membrane-type photonic crystal waveguides," Opt. Express **11**, 2927 (2003), http://www.opticsinfobase.org/abstract.cfm?URI=oe-11-22-2927.
28. J.D. Jackson, Classical electrodynamics. 3rd ed (John Wiley & Sons, Inc., Hoboken, NJ,1999).
29. H.C. Van de Hulst, *Light scattering by small particles* (Dover Publications. Inc., New York, NY,1981).
30. A.F. Koenderink, M. Kafesaki, B.C. Buchler, and V. Sandoghdar, "Controlling the resonance of a photonic crystal microcavity by a near-field probe," Phys. Rev. Lett. **95**, 153904-153901 (2005).
31. L. Aigony, et al., "Polarization effects in apertureless scanning near-field optical microscopy: An experimental study," Opt. Lett. **24**, 187-189 (1999).
32. M. Labardi, et al., "Highly efficient second-harmonic nanosource for near-field optics and microscopy," Opt. Lett. **29**, 62-64 (2004).

1. Introduction

Highly confined optical modes, made possible by the large index contrast in Silicon On Insulator (SOI) or semiconductor air-bridge platforms, have allowed for the development of a variety of compact and efficient photonic devices [1]. Recent SOI photonic devices include optical switches and modulators in microring resonators [2, 3], Mach-Zhender interferometers [4], and photonic crystal cavities [5, 6]. Optical buffers based on the large group index in photonic crystals [6] and Stimulated Raman Scattering (SRS) [7] have been shown experimentally. Raman gain [8-10] and lasing [11, 12] as well as efficient frequency conversion [13] have also been recently demonstrated. The efficiency of these processes relies on the high concentration of optical intensity in the sub-micron-sized silicon core.

With the recent success of such highly integrated sub-micron scale photonic structures comes the need for improved optical characterization techniques to better understand and design future devices. Of particular interest is the measurement of local near field profiles of these devices. Here the highly confined nature of light in these devices makes local field measurements particularly challenging. Because light is confined to non-radiating guided modes and mode features are often smaller than the free space diffraction limit, conventional far field microscopy cannot resolve the local characteristics of guided modes. Therefore there has been much interest in the use of Near-field Scanning Optical Microscopy (NSOM) to observe the local nature of guided modes in photonic devices. NSOM measures the optical near field by scanning a sub-wavelength-sized probe in the vicinity of an evanescent field near the sample's surface.

Previous near field measurement techniques suffer from either poor aperture-limited resolution or poor collection efficiency. Traditional aperture NSOM techniques typically use tapered optical fibers (often metal coated) to collect light from the evanescent field through a sub-wavelength sized aperture [14-17]. Measuring the power collected as a function of probe

#75030 - $15.00 USD Received 14 September 2006; revised 5 October 2006; accepted 6 October 2006

position creates an image of the local evanescent field. This technique has been used to observe confinement and guiding in micron-sized semiconductor waveguides and transverse optical decay lengths as small as λ/7 in the near infrared have been reported [17]. These measurements are challenging since NSOM probes are typically metal coated and thus the probe size is about twice that of the physical aperture. This prevents the aperture from moving close to the sides of the waveguide to measure short transverse optical decay lengths. Additionally, the resolution of these NSOM measurements is limited by the aperture size which is typically no smaller than λ/10. This lower bound on the aperture size is related to the transmission through sub-wavelength-sized holes which falls as $(r/\lambda)^4$ where r is the aperture radius [18]. Apertureless NSOM (a-NSOM), also known as scattering NSOM (s-NSOM), offers several advantages over traditional aperture NSOM. In s-NSOM a sharp metal or dielectric probe scatters some of the local evanescent field into the far field where it can be detected [19-21]. Compared to aperture NSOM probes, s-NSOM probes are generally more robust, inexpensive, and easy to fabricate. The main advantage of such systems, relative to NSOM, is that since light is not collected through the probe, probe diameters can be orders of magnitude smaller than aperture NSOM probes and still generate measurable signals. This greatly increases the spatial resolution of the optical measurements. Since the entirety of the s-NSOM probe is sensitive to the local field (unlike metal coated NSOM probes which only collect light through the aperture at the probe center), they can be used to measure the field very close to the sides of the waveguide. Applying the s-NSOM technique to photonic devices, however, is challenging. Scattered light is often collected in the far field from multiple sources including defects along the waveguide. Separating light scattered from the probe and that scattered from these defects requires complex heterodyne interferometric measurement techniques [22, 23] similar to those used in time-resolved NSOM measurements [24].

In this paper we present a new type of apertureless NSOM: Transmission-based Near-field Scanning Optical Microscopy (TraNSOM), which offers both high resolution imaging and high collection efficiency, eliminating the need for interferometric measurements or far-field collection optics. We achieve this high resolution and improved collection efficiency by measuring the transmission of light through a device where the mode is disturbed by a metallic Atomic Force Microscope (AFM) probe. By disturbing the mode, some of the light confined in the guided mode is coupled to radiation modes (scattering) or absorbed by the probe. The amount of scattering and absorption is related to the local magnitude of the optical near field. Thus, by measuring the transmission as we scan the AFM probe, we construct an image of the optical near field. In contrast to previous s-NSOM techniques we achieve much larger collection efficiency since almost *all* the light scattered and absorbed contributes the measured drop in transmission. A similar technique was recently used to map the mode of an optical resonator, however, reported images showed a resolution of only about 200 nm in the near-IR which is on the same order as NSOM techniques [25]. Using a commercial AFM as a TraNSOM we make the first quantitative measurements of highly confined mode profiles in SOI waveguides which show a transverse optical decay length of λ/15 for the fundamental quasi-TM mode.

2. Experiment

We fabricate sub-micron scale silicon waveguides on an SOI wafer with a 1 micron buried oxide layer. Using a series of thermal oxidation steps the silicon is thinned to a thickness of about 250 nm covered with about 150 nm of thermal oxide. The waveguides are then patterned using electron beam lithography and etched using inductively coupled plasma etching leaving a silicon core approximately 520 nm wide at its base and 250 nm tall covered on top with about 150 nm of thermal oxide. A side wall angle of 79^o is estimated from the waveguide width at the top and bottom measured using a scanning electron microscope. The waveguides are air clad with the exception of the input and output where we adiabatically narrow the width of the waveguides to about 120 nm and cover them with 2 micron tall by 8

#75030 - $15.00 USD Received 14 September 2006; revised 5 October 2006; accepted 6 October 2006

micron wide waveguides made of photoresist which we fabricate using contact lithography. This increases the coupling efficiency and selectivity for the quasi-TE mode [26, 27]. Using an in-line polarization controller to minimize or maximize the output we can selectively excite either the quasi-TM or quasi-TE mode respectively. We measure a total transmittance for quasi-TE to be about 20 times larger than for quasi-TM.

The experimental TraNSOM setup consists of a photonic chip bonded to input and output optical fibers and placed under a commercial AFM. A schematic of this setup is shown in Fig. 1. As a light source we use about 80 mW of unpolarized amplified spontaneous emission (ASE) output from an Erbium Doped Fiber Amplifier (EDFA) sent through a tunable grating filter set to 1532 nm to match the peak of the ASE. The output of the filter is sent through an in-line polarization controller to a cleaved optical fiber which is coupled to the waveguide input and bonded to a microscope slide using a low-shrink UV curable epoxy (Dymax OP-4-20641). A cleaved optical fiber is also coupled to the waveguide output and bonded to the microscope slide. The output fiber is sent to a photo-detector and power meter. We then place the packaged photonic device in a Dimension 3100 AFM with an acoustic enclosure. Using a PtIr coated probe from Nanosensors we image the device in intermittent contact or "tapping" mode. The analog output of the power meter is sent to voltage pre-amplifier with a 30 Hz low pass filter to reduce high frequency noise. The output of the voltage pre-amplifier is sent to the auxiliary input of the AFM which simultaneously records the topography and transmission through the device as the probe is scanned over the sample.

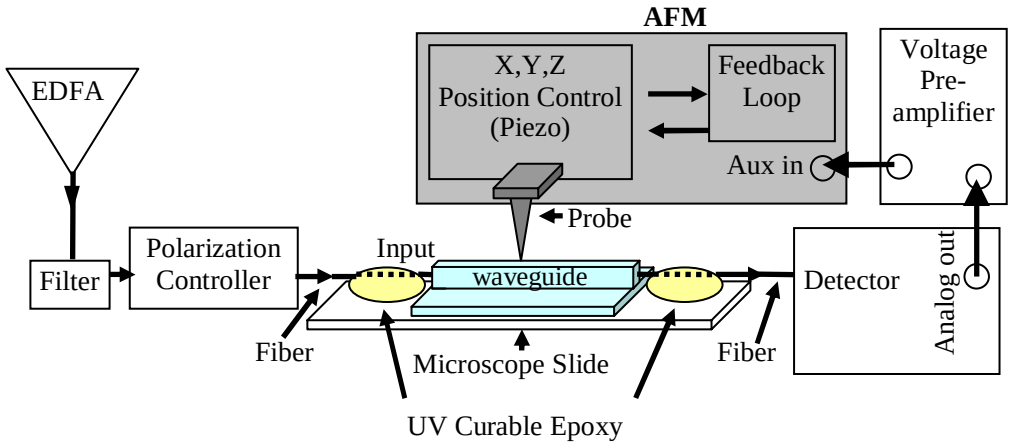

Fig. 1. Experimental setup for TraNSOM measurements.

3. TraNSOM signal

To quantitatively understand what is measured by the change in transmission, we analyze the scattering and absorption induced by the near-field probe. According to scattering theory [28, 29], to first order the power scattered and absorbed is the result of damped dipole radiation induced by the incident electric field. The magnitude of the induced dipole depends on the probe material, geometry, and the relative polarization and magnitude of the incident electric field. By modeling the probe as a cone, one can choose the principal axes of the cone as a Cartesian basis such that $\hat{y}$ is along the cone axis and $\hat{x}$ and $\hat{z}$ are in the plane perpendicular to the cone axis (see Fig. 2). Since the polarizability is diagonal in this basis we can write the total power lost (P_{ext}) as the sum of the power lost to absorption (P_{abs}) and scattering (P_{sca}):

#75030 - $15.00 USD Received 14 September 2006; revised 5 October 2006; accepted 6 October 2006

$$P_{ext} = P_{abs} + P_{sca} = Q_{ext\perp}\frac{1}{2}\sqrt{\frac{\mu_0}{\varepsilon_0}}\int_A |E_x|^2 da + Q_{ext\parallel}\frac{1}{2}\sqrt{\frac{\mu_0}{\varepsilon_0}}\int_A |E_y|^2 da + Q_{ext\perp}\frac{1}{2}\sqrt{\frac{\mu_0}{\varepsilon_0}}\int_A |E_z|^2 da\,, \quad (1)$$

where A is the cross sectional area of the scattering probe, $Q_{ext\perp}$ is the extinction efficiency for the field perpendicular to the probe axis, and $Q_{ext\parallel}$ is the extinction efficiency for the field parallel to the probe axis. The extinction efficiency is defined as the scattering cross section plus the absorption cross section divided by the geometric cross section [29]. This is equivalent to the total power scattered and absorbed normalized to the power incident on the probe. Scattering efficiencies much less than one indicate that light passes relatively unimpeded through the object. It has been shown by several sources [30-32] that the probe-field interaction is dominated by the polarization component along the tip axis. Appling this condition ($Q_{ext\parallel} >> Q_{ext\perp}$) we can approximate the total power loss as:

$$P_{ext} \approx Q_{ext\parallel}\frac{1}{2}\sqrt{\frac{\mu_0}{\varepsilon_0}}\int_A |E_y|^2 da\,. \quad (2)$$

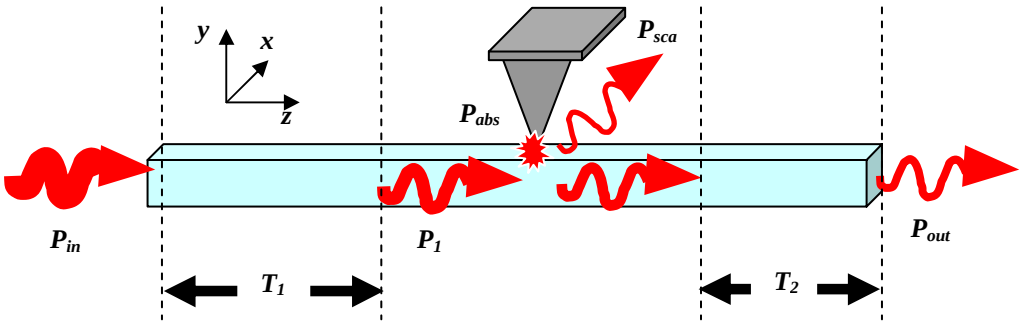

Fig. 2. Model of the TraNSOM measurement where P_{in} is the power input from the source, T_1 is the transmittivity between the source and the probe, P_{abs} is the power absorbed by the probe, P_{sca} is the power scattered by the probe, T_2 is the transmittivity between the probe and the detector, and P_{out} is the power detected at the output.

We now relate the measured transmission signal to the local electric field. We can write the transmitted power measured at the detector (P_{out}) in terms of the power input from the source (P_{in}), the total transmittance between the source and the probe position (T_1) and the probe position and detector (T_2), and the power lost to absorption and scattering by the probe (P_{ext}) (see Fig. 2) as

$$P_{out} = T_1 T_2 P_{in}\left(1 - \frac{P_{ext}}{P_1}\right), \quad (3)$$

where we have defined the power in the waveguide immediately before the probe as $P_1 \equiv T_1 P_{in}$ which is equivalent to an integral of the pointing flux through an infinite plane just before the probe $\left(P_1 = \frac{1}{2}\int_\infty \left(\vec{E}\times\vec{H}\right)\cdot\hat{z}\, da\right)$. In the absence of the probe the measured power follows from (3):

$$P_{out0} = T_1 T_2 P_{in}\,. \quad (4)$$

We define the measured signal (ΔT) in terms of the measured transmission with and without the probe:

#75030 - $15.00 USD Received 14 September 2006; revised 5 October 2006; accepted 6 October 2006

$$\Delta T \equiv 1 - \frac{P_{out}}{P_{out\,0}} = \frac{P_{ext}}{P_1} \approx \frac{Q_{ext\|}\sqrt{\frac{\mu}{\varepsilon}}\int_A |E_y|^2\, da}{\int_\infty \left(\vec{E}\times\vec{H}\right)\cdot\hat{z}\, da}. \quad (5)$$

Therefore the measured quantity is related to the square of the local electric field normalized to the local power in the mode.

4. Measurement and Simulation

Using the experimental setup described above we measure the topography and optical mode of a sub-micron-sized SOI waveguide. Figures 3(a) and (b) show the simultaneously recorded topographic and TraNSOM image of the quasi-TM mode scanned over a 2x2 micron region. We use a 2-line interpolation in WSxM to help remove high frequency noise in the images. Notice that the small pillars to the left and right of the waveguide resulting from micro-masking in the fabrication process do not appear in the optical image since the optical field is confined only to the waveguide.

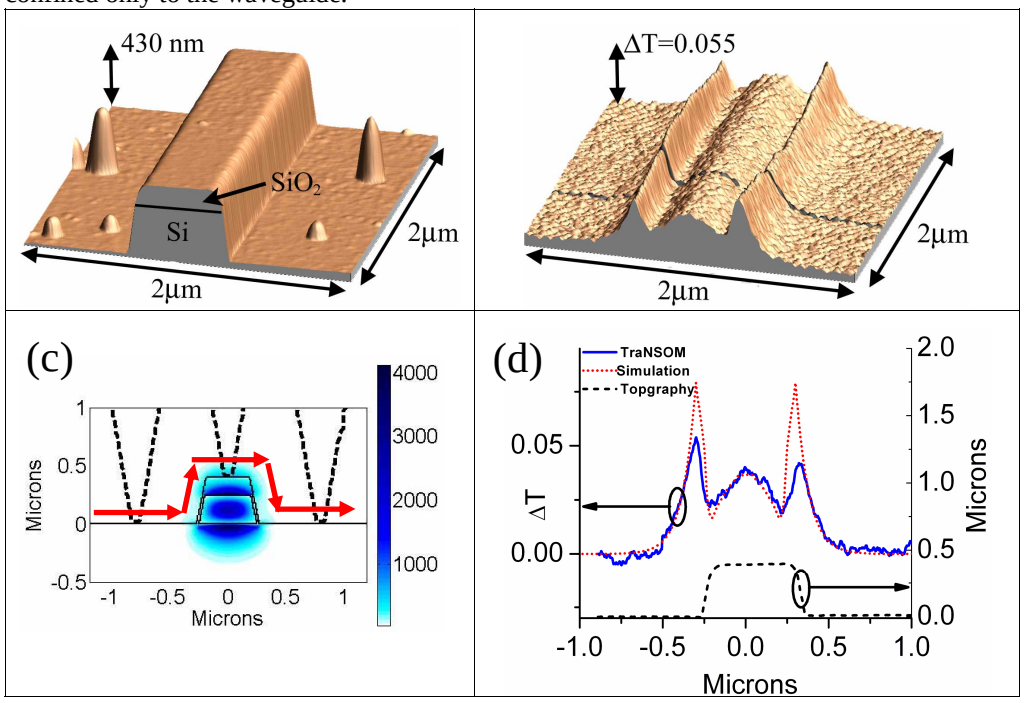

Fig. 3. (a) AFM image of the SOI waveguide (b) simultaneously recorded TraNSOM image of the fundamental quasi-TM mode (c) simulated major component ($|E_y|^2$) of the fundamental quasi-TM mode. Dashed lines show the outline of the probe at three positions. Bold arrows show the path of the probe convolution. (d) Solid line shows the measured TraNSOM signal taken along the solid line in (b). Dashed line shows the simultaneously measured topography. Dotted line shows the probe-field convolution for all three polarization components according to (1) with $Q_{ext|} = 6.4$ and $Q_{ext\perp} = 0.08$.

We verify the measurement technique by comparing the measured mode profile to calculated results and determine the transverse optical decay length for the quasi-TM mode. Since the probe is most sensitive to the field polarized along the cone axis. We plot the major component of the quasi-TM mode ($|E_y|^2$) in Fig. 3(c) calculated using a finite element mode solver and normalized to unit power. The dashed lines outline the probe cross section at three different positions as it is scanned over the waveguide. The probe dimensions are taken from

#75030 - $15.00 USD Received 14 September 2006; revised 5 October 2006; accepted 6 October 2006

the manufacturer specifications of a 10^{o} half angle and 25 nm radius of curvature. Figure 3(d) shows a cross section of the measured ΔT (solid blue) taken along the line shown in Fig. 3(b). The simultaneously measured topography is shown as the dashed black line. The dotted red line in Fig. 3(d) shows the convolution of the probe cross section (A) with the simulated mode profile shown in Fig. 3(c). This convolution was performed for all three field components and weighted by $Q_{ext\|}$ and $Q_{ext\perp}$ (given below) according to (1). We measure the transverse optical decay length by analyzing the evanescent field measured to the left and right of the waveguide. We fit the evanescent field in Fig. 3(d) to an exponential which decays as $\exp(-|x|/\xi)$ where x is the distance from the waveguide core and ξ is the transverse optical decay length. From the fit we measure this quantity to be 100 ± 12 nm (~λ/15), where the error represents the 95% confidence interval. This result compares well with the convolution of the probe with the calculated mode profile which predicts a transverse optical decay length of 70 nm.

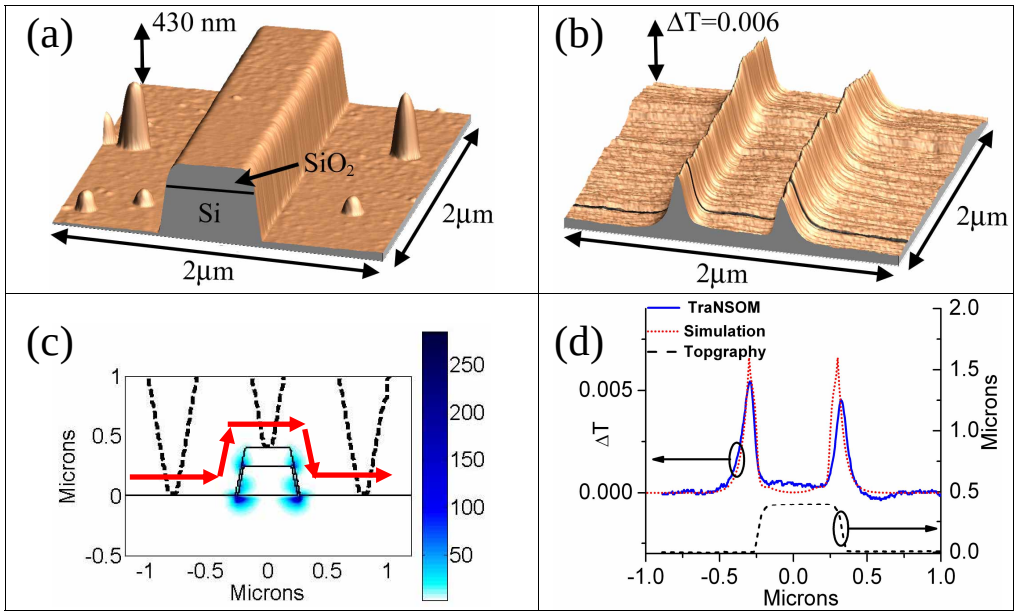

Fig. 4. (a) AFM image of the SOI waveguide (b) simultaneously recorded TraNSOM image of the fundamental quasi-TE mode (c) Simulated minor component ($|E_y|^2$) of the fundamental quasi-TE mode. Dashed lines show the outline of the probe at three positions. Bold arrows show the path of the probe convolution. (d) Solid line shows the measured TraNSOM signal taken along the solid line in (b). Dashed line shows the simultaneously measured topography. Dotted line shows the probe-field convolution for all three polarization components according to (1) with $Q_{ext|} = 6.4$ and $Q_{ext\perp} = 0.08$.

To confirm we are indeed predominantly measuring the field polarized along the probe axis, we compare a measurement of the quasi-TE mode with its calculated minor field component ($|E_y|^2$). Figures 4(a) and (b) show the simultaneously recorded topographic and TraNSOM image of the quasi-TE mode scanned over the same 2x2 micron region as Fig. 3(a) and (b). Figure 4(c) shows the minor component $|E_y|^2$ for the quasi-TE mode normalized to unit power and the path of the probe convolution. Note that since this is the minor field component, the magnitude of the field is ten times smaller than the major component of the quasi-TM mode (Fig. 3(c)) and concentrated near the waveguide corners which is typical in high-index-contrast waveguides. This is in agreement with the measured mode profile in Fig.

#75030 - $15.00 USD Received 14 September 2006; revised 5 October 2006; accepted 6 October 2006

4(b) which shows the field is concentrated near the edges of the waveguide and shows a ten fold decrease in the magnitude of the measured signal compared to the quasi-TM mode (note the scale difference of ΔT in Figs. 3(b) and 4(b)). Figure 4(d) shows a cross section of the measured ΔT (solid blue) taken along the line shown in Fig. 4(b). The simultaneously measured topography is shown as the dashed black line. The dotted red line in Fig. 4(d) shows the convolution of the probe cross section (A) with the simulated mode profiles shown in Fig. 4(c) weighted by $Q_{ext\|}$ and $Q_{ext\perp}$. Similarly to the analysis of the major field component of the quasi-TM mode, we analyze the transverse optical decay length of the *minor* field component ($|E_y|^2$) of the quasi-TE mode. Fitting the exponential decay to the left and right of the waveguide we measure the minor field transverse optical decay length to be 49 ± 9 nm (~λ/30), which compares very well with the 46 nm decay length predicted by our simulations. To our knowledge, these transverse optical decay lengths for the quasi-TM and quasi-TE modes are the shortest measured for waveguides in the near infrared and are a result of the high index contrast between Si and air.

We determine the quantitative extinction efficiency of the probe for two orthogonal polarizations by fitting the measured data to the calculated probe-field convolution. The values of $Q_{ext\|} = 6.4 \pm 0.5$ and $Q_{ext\perp} = 0.08 \pm 0.05$ are calculated by performing a least squares fit of the simulated probe-field convolution to the measured data simultaneously for the quasi-TE and quasi-TM data over the regions that are topographically flat. The results of this fit are plotted as the dotted lines in Figs. 3(d) and 4(d). The fact that $Q_{ext\|}$ is two orders of magnitude larger than $Q_{ext\perp}$ confirms the assumption in Section 3 that for this probe geometry, the field along the probe axis (E_y) dominates the measured signal (i.e.: $Q_{ext\|} >> Q_{ext\perp}$). Note that the simulated data over-estimates the probe-field interaction near the upper corners of the waveguide since the fabricated waveguide has rounded corners with about a 60 nm radius of curvature, as seen in the AFM images (Figs. 3(a) and 4(a)), which keep the probe farther from the waveguide core than is predicted from the sharp cornered simulations shown in Figs. 3(c) and 4(c).

5. Conclusions

We demonstrate a novel technique for measuring sub-micron optical features of highly confining photonic structures. Using this new high resolution apertureless technique we measure a transverse optical decay length for the quasi-TM mode of λ/15 which, to our knowledge, is the shortest decay length measured in near infrared waveguides. As opposed to previous near field measurement techniques, this technique enables both high collection efficiency and high resolution and therefore does not require any far field collection optics, interferometric measurements, or expensive aperture probes.

Acknowledgments

The authors would like to thank Kit Umbach and Leon Bellan for the use of equipment and their helpful insight into scanned probe microscopy. Research support is gratefully acknowledged from the National Science Foundation Center on Materials and Devices for Information Technology Research (CMDITR), DMR-0120967,.,the Cornell Center for Material Research, and the National Science Foundation's CAREER Grant No. 0446571. This work was performed in part at the Cornell NanoScale Facility, a member of the National Nanotechnology Infrastructure Network, which is supported by the National Science Foundation (Grant ECS 03-35765) and we made use of STC shared experimental facilities supported by the National Science Foundation under Agreement No. ECS-9876771.

#75030 - $15.00 USD Received 14 September 2006; revised 5 October 2006; accepted 6 October 2006